2021 SCEC Annual Report

Modeling of the 2019 M7.1 Ridgecrest, CA, Earthquake, Including a Data-constrained Fault Zone

Report for SCEC Award 21111

PI: Dr. Kim B. Olsen

Institution: Department of Geological Sciences, San Diego State University, San Diego, CA 92182-1020

Publications and Reports:

Yeh, T-Y., and K.B. Olsen (2021). 3D wave propagation simulations of the 2019 M7.1 Ridgecrest, CA, Earthquake, *Seism. Res. Lett.* **92**, 2B, 1413.

Yeh, T-Y., and K.B. Olsen (2021). 3D wave propagation simulations of the 2019 M7.1 Ridgecrest, CA, Earthquake, *SCEC AM*, Poster #49 (scec.org/meetings/2021/am/poster/049)

Summary

We continue our 3D deterministic modeling of the July 2019 M7.1 Ridgecrest, CA, earthquake. We use the GPU-enabled (Cui et al., 2013) version of AWP (AWP-GPU), and map the contributions to the ground motions from surface topography, Q(f), and small-scale heterogeneities. Inclusion of the effects of the low near-surface material (Vs(min)=300 m/s) is enabled using the discontinuous-mesh version of AWP (Nie et al., 2017). We use kinematic rupture models from source inversion, enriched in higher frequency signal. We include a model of the fault damage zone adapted from Zhou et al. (2022) from ambient noise cross correlation, which generally improves the fit to data, by increasing the peak ground velocities (PGVs, at select sites by more than 50%) and Fourier Amplitude Spectra (FAS). We find that in general, the best fit to the data is obtained by including both the damage zone and a shallow (<700 m) geotechnical layer (GTL). Simulations including nonlinear (plastic) effects following Drucker-Prager rheology shows reduction of PGVs and peak ground accelerations (PGAs) in the fault zone, in particular in the southern end, by up a factor of 2. However, the far-field waves from the M7.1 Ridgecrest earthquake are not significantly affected by plastic effects in the damage zone.

Effect of the M7.1 Ridgecrest Damage Zone on Ground Motions

The detailed velocity structure near the faults that ruptured during the 2019 Ridgecrest Earthquake sequence are not resolved in the SCEC Unified Community Velocity model (UCVM) CVM-S4.26.M01, also known as CVMSI (Small et al., 2017), due to the limited spatial resolution in the Ridgecrest area. In order to investigate the effects of the fault zone structure on the predicted ground motions, we incorporated the near-fault 3D velocity structure inverted from the ambient noise data (Zhou et al., 2022) into the SCEC UCVM (see **Fig. 1**). The 3D S-wave velocity structure of the fault zone was imaged in a domain of the size 50 km (length) by 45 km (width) by 5 km (depth), and we used the empirical relations from Brocher (2005) to compute P-wave speeds and densities. The lowest surface Vs within the imaged fault zone model is around 1100 m/s, as compared to a minimum surface Vs of 1400 m/s in the original UCVM. Smoothing was done along the edges and corners of the replacement domain to remove the sharp contrasts that would cause unrealistic reflections (see **Fig. 2**).

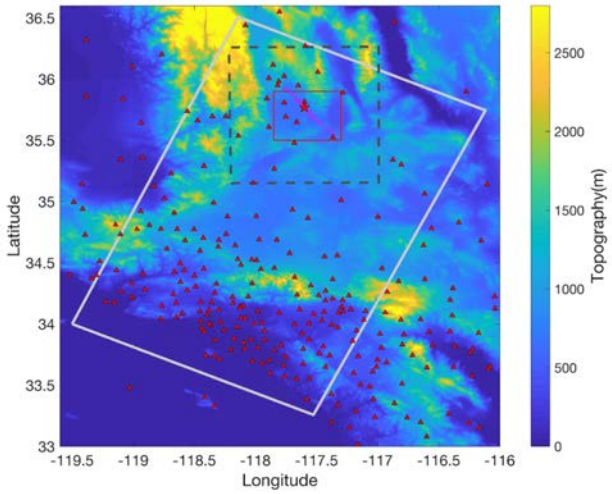

Figure 1. Simulation domain (dashed rectangle). The red triangles show locations of stations providing seismic recordings of the 2019 Ridgecrest M7.1 earthquake. The magenta line depicts the surface projection of the Liu et al. (2019) rupture model. The red box depicts the domain where the fault zone S-wave velocity structure was imaged by Zhou et al. (2022). The large rectangle depicts the domain to be used for wave propagation simulations into the Los Angeles basin. The background shading shows topographic relief.

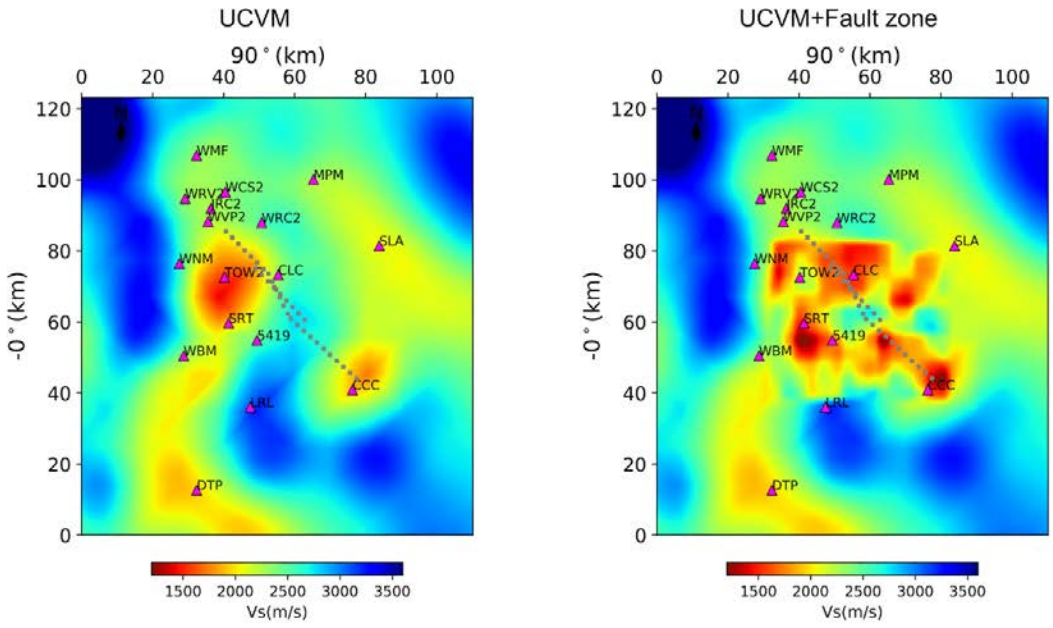

Figure 2. S-wave velocities at the surface without (left) and with (right) incorporating the fault zone structure into SCEC UCVM. Dots depict the surface projection of subfaults of the Liu et al. (2019) rupture model of the M7.1 Ridgecrest event. The triangles are station locations. Note that no geotechnical layers have been added here.

To illustrate the effects of the fault damage zone on the ground motions, **Figure 3** compares the observed ground motions to simulated time histories with and without the damage zone at station CLC (see **Fig. 2** for location). Generally, the fault damage zone improves the fit to data, by increasing PGVs (at select sites by more than 50%) and FAS.

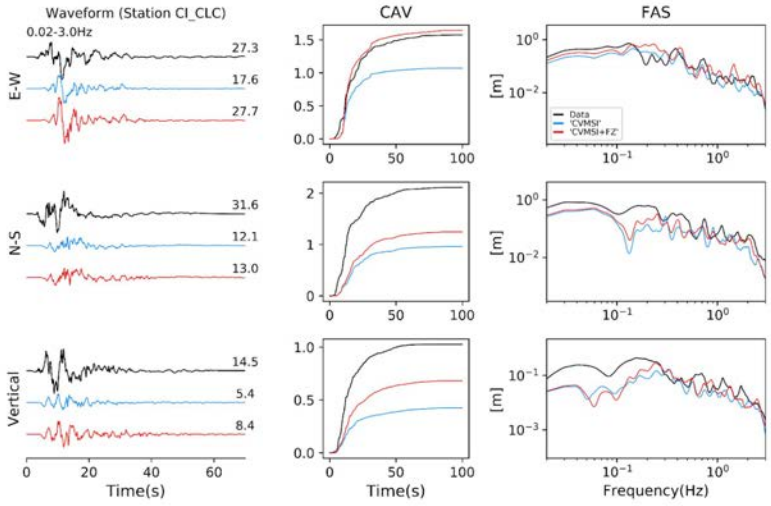

Figure 3. Comparison of observed (black traces) and simulated (red and blue traces) waveforms, cumulative absolute velocity histories (CAV), and FAS for station CLC (see **Fig. 2**). Blue traces were simulated with CVMSI only, and red traces were computed with CVMSI including the fault damage zone structure incorporated. The attenuation model for both solutions is $Qs = 0.075\ Vs\ f^{o}$.

We also tested the effects of a GTL inserted to a depth of 700 m following the formulation of Ely et al. (2010) with the Vs30 model from Wills et al. (2015). **Fig. 4** shows the surface Vs of the simulation domain after including the GTL, and **Figs. 5-6** illustrates the relative effects of the damage zone and GTL. We find that in general, the best fit to the data is obtained by including both the damage zone and the GTL.

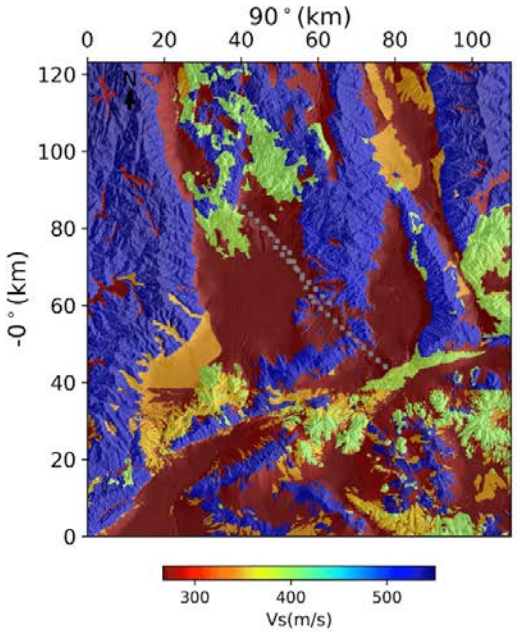

Figure 4. Same as **Figure 2**, but from the model after adding the GTL in the top 700m.

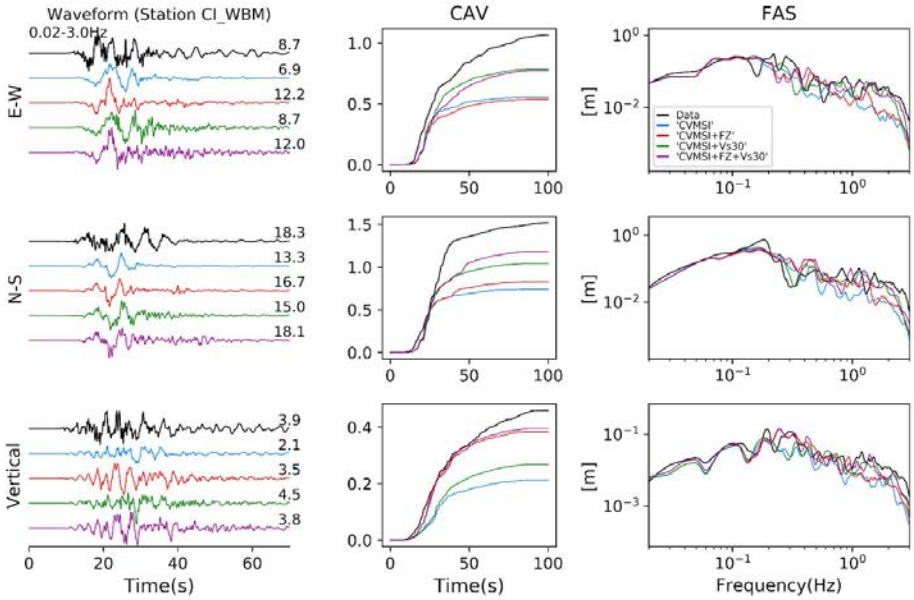

Figure 5. Comparison at station WBM (see **Fig. 2**) of (black) observations, models of (blue) CVMSI only, (red) CVMSI+fault zone, (green) CVMSI+GTL, and (purple) CVMSI+fault zone+GTL. The attenuation model for all solutions is $Qs = 0.075\ Vs\ f^{o}$

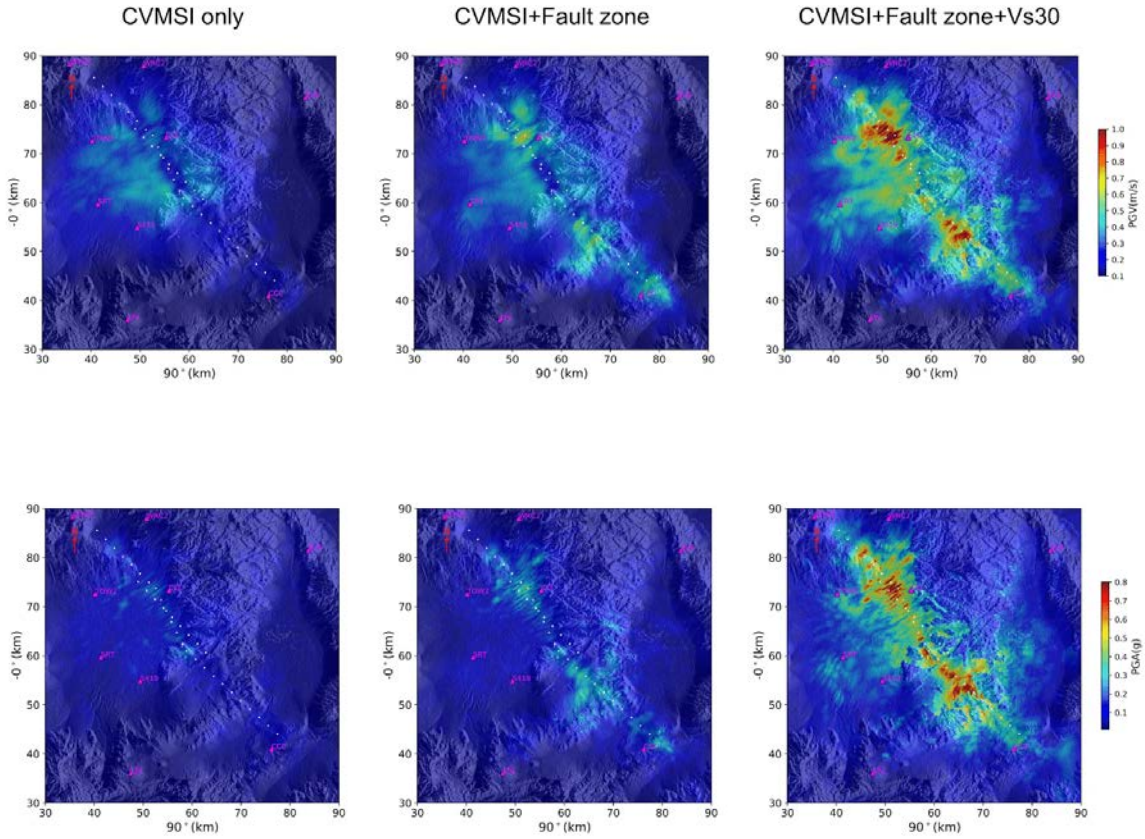

Figure 6. Comparison of (top) PGV and (bottom) PGA computed for models with (left) CVMSI only, (center) CVMSI+fault zone, and (right) CVMSI+Fault zone+GTL. The attenuation model for all solutions is $Qs = 0.075\ Vs\ f^{o}$.

Effects of Nonlinearity

In addition to the linear simulations, we also investigated the nonlinear response of the low velocity material at shallow depth during the M7.1 Ridgecrest event, assuming Ducker-Prager yield conditions. Here, we used the Hoek-Brown failure criterion that provides effective cohesion and a friction angle for the nonlinear simulation (Hoek et al., 2002). We assign Geological Strength Index (GSI) based on local S-wave speed assuming the strength of the rock is proportional to the seismic wave speed. GSI was assigned as follows.

Vs	GSI
<= 300 m/s	20
300 m/s - 500 m/s	20 to 40
500 m/s - 1500 m/s	40 to 90
1500 m/s - 2000 m/s	90 to 100
>= 2000 m/s)	100

As expected, nonlinearity mostly occurs along the fault trace (**Figs. 7-8**). The nonlinear simulation predicts accumulated strain up to about 10^{-3} along the fault. The southeastern end of the fault experiences the largest reduction of ground motions. However, the waveforms computed for near-fault sites from linear and nonlinear calculations are very similar. Based on these results, we do not expect significant nonlinear effects in the far-field waves from the M7.1 Ridgecrest event.

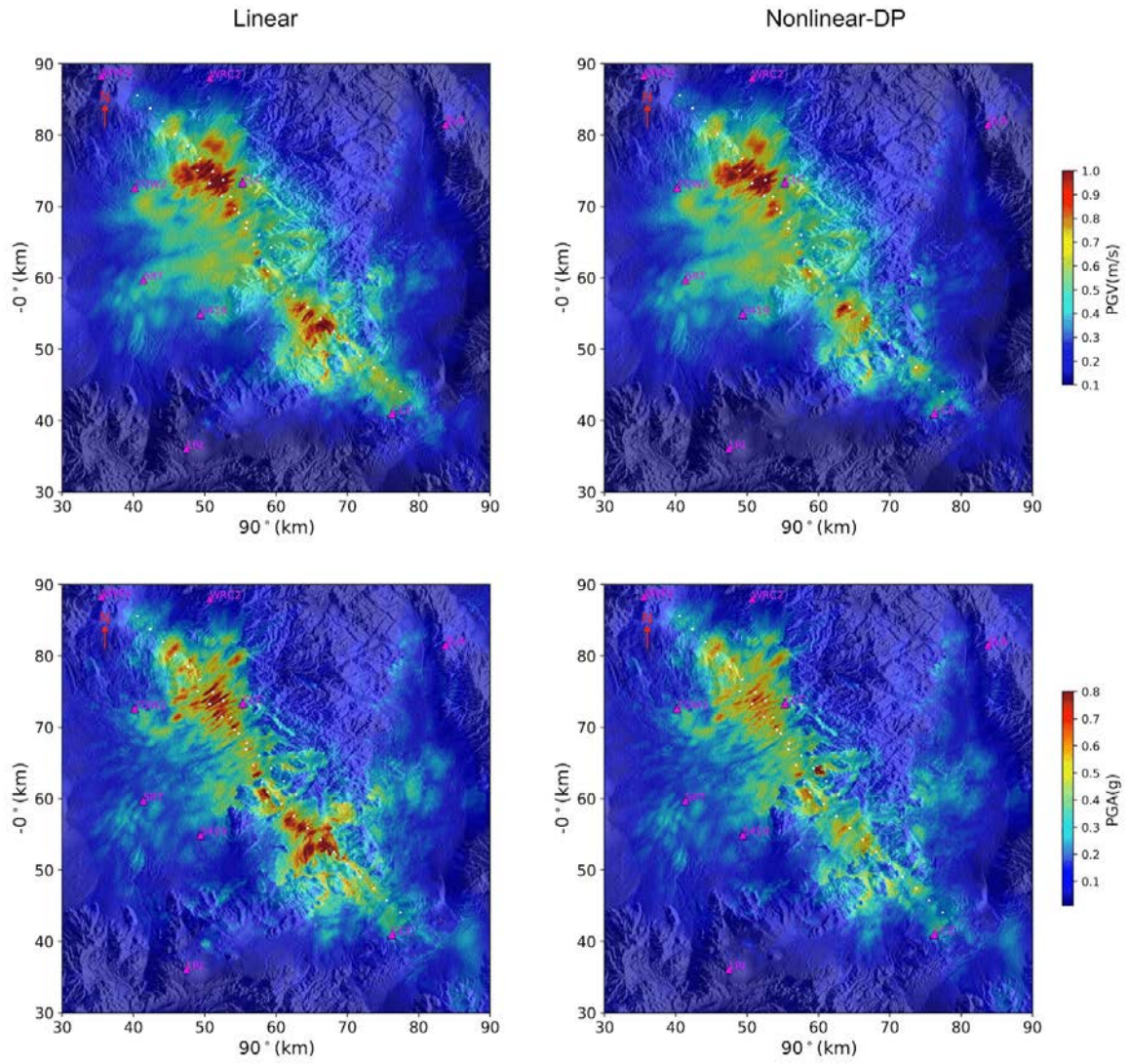

Figure 7. Comparison of (top) PGV and (bottom) PGA computed for models with CVMSI+Fault zone+GTL for (left) linear rheology and (right) nonlinear (Drucker-Prager) rheology. All solutions used Qs = 0.075 Vs f^{o}.

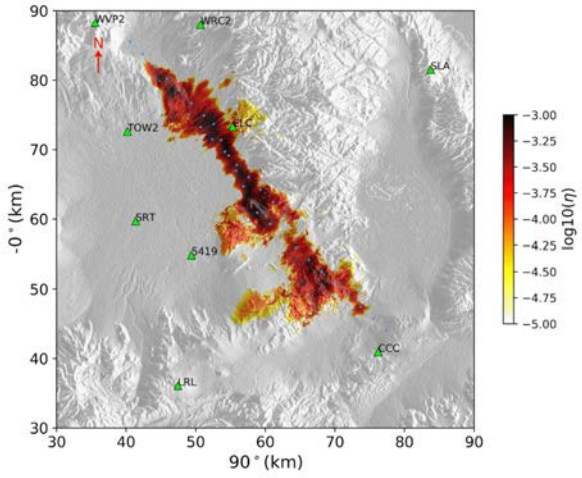

Figure 8. Cumulative strain from a simulation using Drucker-Prager rheology.

References

Brocher, T. M. (2005). Empirical Relations between Elastic Wavespeeds and Density in the Earth's Crust. *Bulletin of the Seismological Society of America, 95*(6), 2081-2092. https://doi.org/10.1785/0120050077

Cui, Y., Poyraz, E., Olsen, K. B., Zhou, J., Withers, K., Callaghan, S., et al. (2013, 17-22 Nov. 2013). *Physics-based seismic hazard analysis on petascale heterogeneous supercomputers.* Paper presented at the SC '13: Proceedings of the International Conference on High Performance Computing, Networking, Storage and Analysis.

Ely, G. P., Jordan, T., Small, P., & Maechling, P. J. (2010). *A VS30-derived nearsurface seismic velocity model.* Paper presented at the Abstract S51A-1907, Fall Meeting.

Hoek, E., Carranza-Torres, C., & Corkum, B. (2002). Hoek-Brown failure criterion-2002 edition. *Proceedings of NARMS-Tac, 1*(1), 267-273.

Liu, C., Lay, T., Brodsky, E. E., Dascher-Cousineau, K., & Xiong, X. (2019). Coseismic Rupture Process of the Large 2019 Ridgecrest Earthquakes From Joint Inversion of Geodetic and Seismological Observations. *Geophysical Research Letters, 46*(21), 11820-11829. https://agupubs.onlinelibrary.wiley.com/doi/abs/10.1029/2019GL084949

Nie, S., Wang, Y., Olsen, K. B., & Day, S. M. (2017). Fourth-Order Staggered-Grid Finite-Difference Seismic Wavefield Estimation Using a Discontinuous Mesh Interface (WEDMI)Fourth-Order Staggered-Grid Finite-Difference Seismic WEDMI. *Bulletin of the Seismological Society of America, 107*(5), 2183-2193. https://doi.org/10.1785/0120170077

O'Reilly, O., Yeh, T. Y., Olsen, K. B., Hu, Z., Breuer, A., Roten, D., & Goulet, C. A. (2021). A High-Order Finite-Difference Method on Staggered Curvilinear Grids for Seismic Wave Propagation Applications with Topography. *Bulletin of the Seismological Society of America*. https://doi.org/10.1785/0120210096

Small, P., Gill, D., Maechling, P. J., Taborda, R., Callaghan, S., Jordan, T. H., et al. (2017). The SCEC Unified Community Velocity Model Software Framework. *Seismological Research Letters, 88*(6), 1539-1552. https://doi.org/10.1785/0220170082

Wills, C. J., Gutierrez, C. I., Perez, F. G., & Branum, D. M. (2015). A Next Generation VS30 Map for California Based on Geology and Topography. *Bulletin of the Seismological Society of America, 105*(6), 3083-3091. https://doi.org/10.1785/0120150105

Withers, K. B., Olsen, K. B., & Day, S. M. (2015). Memory-Efficient Simulation of Frequency-Dependent QMemory-Efficient Simulation of Frequency-Dependent Q. *Bulletin of the Seismological Society of America, 105*(6), 3129-3142. https://doi.org/10.1785/0120150020

Zhou, Z., M. Bianco, P. Gerstoft, and K.B. Olsen (2022). High-resolution Imaging of Complex Shallow Fault Zones Along the July 2019 Ridgecrest Ruptures, Geophys. Res. Lett. 49, e2021GL095024. https://doi.org/10.1029/2021GL095024.